591781

Final Technical Report
(NASA Award No. NAG3-1879 22 May 1996 – 21 May 2000)

COMBUSTION SYNTHESIS OF FULLERENES AND FULLERENIC NANOSTRUCTURES IN MICROGRAVITY

Jack B. Howard*, Principal Investigator

Department of Chemical Engineering
Massachusetts Institute of Technology
Cambridge, Massachusetts

SUBMITTED TO: NASA Center for Aerospace Information
ATTN: Accessioning Department
7121 Standard Drive
Hanover, MD 21076-1320

John E. Brooker — Technical/Scientific Officer
NASA Glenn Research Center
21000 Brookpark Road, MS 500-115
Cleveland, OH 44135-3191

Ray Galgas — Awarding Contract Officer
NASA Glenn Research Center
21000 Brookpark Road, MS 500-309
Cleveland, OH 44135-3191

*ADDRESS MIT 66-454
77 Massachusetts Avenue
Cambridge, MA 02139

Telephone: 617-253-4574
Fax: 617-258-5042
e-mail: jbhoward@mit.edu

Summary

Fullerenes, the recently discovered curved carbon species including molecules such as C_{60} and C_{70} and nanostructures such as tubes, spheroids and other shapes, are of intense scientific interest and promising potential for a range of applications. Fullerenes can be formed in flames under suitable conditions and the yields can be large enough to support interest in combustion reactors for large-scale fullerenes production. The understanding of fullerenes formation in flames is at an early stage where there is much need for basic combustion research. Experiments are needed to determine the range of fullerene types and yields formed under different conditions, and mechanistic understanding of the results is needed as a basis for extrapolation to practical operating conditions. One of the independent variables of interest is gravity. Through natural convection, gravity is expected to influence, to various extents, the structure of many of the flames of interest in fullerenes formation, and the resulting effects on the types and yields of fullerenes produced need to be understood.

The objectives of the proposed research were to determine the effects of gravity on fullerenes formation in flames and, based on the observed effects, to develop fundamental understanding of fullerenes formation and to identify engineering principles for fullerenes production. The research method consisted of the operation of laminar diffusion flames under normal- and reduced-gravity conditions, and the collection from the flames and subsequent analysis of condensables including any fullerenes present, using coupled high performance liquid chromatography/mass spectrometry and high resolution transmission electron microscopy. The focus included fullerene molecules C_{60} and C_{70} and fullerenic nanostructures including tubes,

spherules and other shapes. The normal-gravity experiments were performed at MIT and complementary reduced-gravity experiments were to have been contributed by NASA.

The independent variables of interest are gravity, fuel type, fuel/oxygen ratio, pressure, gas velocity at burner, and diluent type and concentration. Given the large number of variable and the absence of data on either fullerene formation in diffusion flames or gravitational effects on fullerenes formation in diffusion or premixed flames, the first part of the work was exploratory while the later part involved detailed study of the most interesting mechanisms. Different sets of values of the independent variables were covered in experiments at MIT and a limited set of conditions was to have been studied under reduced-gravity conditions at NASA.

Samples of condensable material from laminar low pressure benzene/argon/oxygen diffusion flames were collected and analyzed by high-performance liquid chromatography to determine the yields of fullerenes, and by high-resolution transmission electron microscopy (HRTEM) to characterize the fullerenic material, i.e. curved-layer nanostructures, on and within the soot particles. The highest concentration of fullerenes was always detected just above the visible stoichiometric surface of a flame. The percentage of fullerenes in the condensable material increases with decreasing pressure. The overall highest amount of fullerenes was found for a surprisingly high dilution of fuel with argon. A comparison of the flames with the same cold gas velocity of fuel and oxygen showed a strong dependence of fullerene content on flame length. A shorter flame, resulting from higher dilution or lower pressure, favors the formation of fullerenes rather than soot, and the amount of soot and precursors of both soot and fullerenes is less at lower pressure and higher dilution. This behavior indicates a stronger correlation of fullerene

consumption to the total amount of soot than of fullerene formation to precursor concentration. The maximum flame temperature seems to be of minor importance in fullerene formation. The HRTEM analysis of the soot showed an increase of the curvature of the carbon layers, and hence increased fullerenic character, with increasing distance from the burner up to the point of maximum fullerene concentration. After this maximum, where soot and fullerenes are consumed by oxidation, the curvature decreases. In addition to the soot, the samples included fullerenic nanostructures such as tubes and spheroids including highly-ordered multilayered or onion-like structures. The soot itself shows highly ordered regions that appear to have been cells of ongoing fullerenic nanostructure formation.

Introduction

Fullerenes, a new form of carbon, were discovered in 1985 [1] in graphite vaporization under inert gas at low pressure. Fullerenes have many properties different from either diamond or graphite. Potential applications include superconductors, sensors, catalysts, optical and electronic devices, polymer composites, high energy fuels, and biological and medical materials. Other interesting classes of fullerenic or curved-layer carbon, as opposed to graphitic or planar-layer carbon, that can also be found in fullerene producing systems, are nanostructures having tubular, spheroidal, or other shapes and consisting of onion-like or nested closed shells [2,3,4,5], and soot particles having considerable curved-layer content [6,7].

Fullerenes can also be formed in premixed hydrocarbon flames under reduced pressure and fuel-rich conditions. They were first detected in flames in ionic form by the Homann group [8,9] and later isolated in macroscopic quantities by Howard et al. [10,11,12]. Higher fullerenes [13], derivatives containing hydrogen and oxygen [14,15], and fullerenic nanostructures [4,5,16] and soot [6,7] have also been detected in premixed flames.

The highest yields of fullerenes in flames are obtained under conditions of substantial soot formation. To understand the mechanism of fullerene formation and enable the design of practical combustion systems for large-scale fullerene production, more information on fullerene yields under various conditions is needed. Little work has been reported on the formation of fullerenes in diffusion flames.

To explore the effects of pressure and diluent gas on fullerene yields in diffusion flames, samples of condensable material from diffusion flames under different conditions were collected and analyzed to determine the concentration of fullerenes, to identify fullerenic nanostructures, and to characterize the curvature of the carbon layers in the soot.

Experimental

The experimental setup for the burning of low pressure laminar diffusion flames of benzene vapor diluted with argon in oxygen is shown in Fig. 1. The vertically-adjustable burner consists of a 10-mm-ID fuel outlet tube surrounded by a 30.5-cm-diameter porous bronze plate through which oxygen is fed.

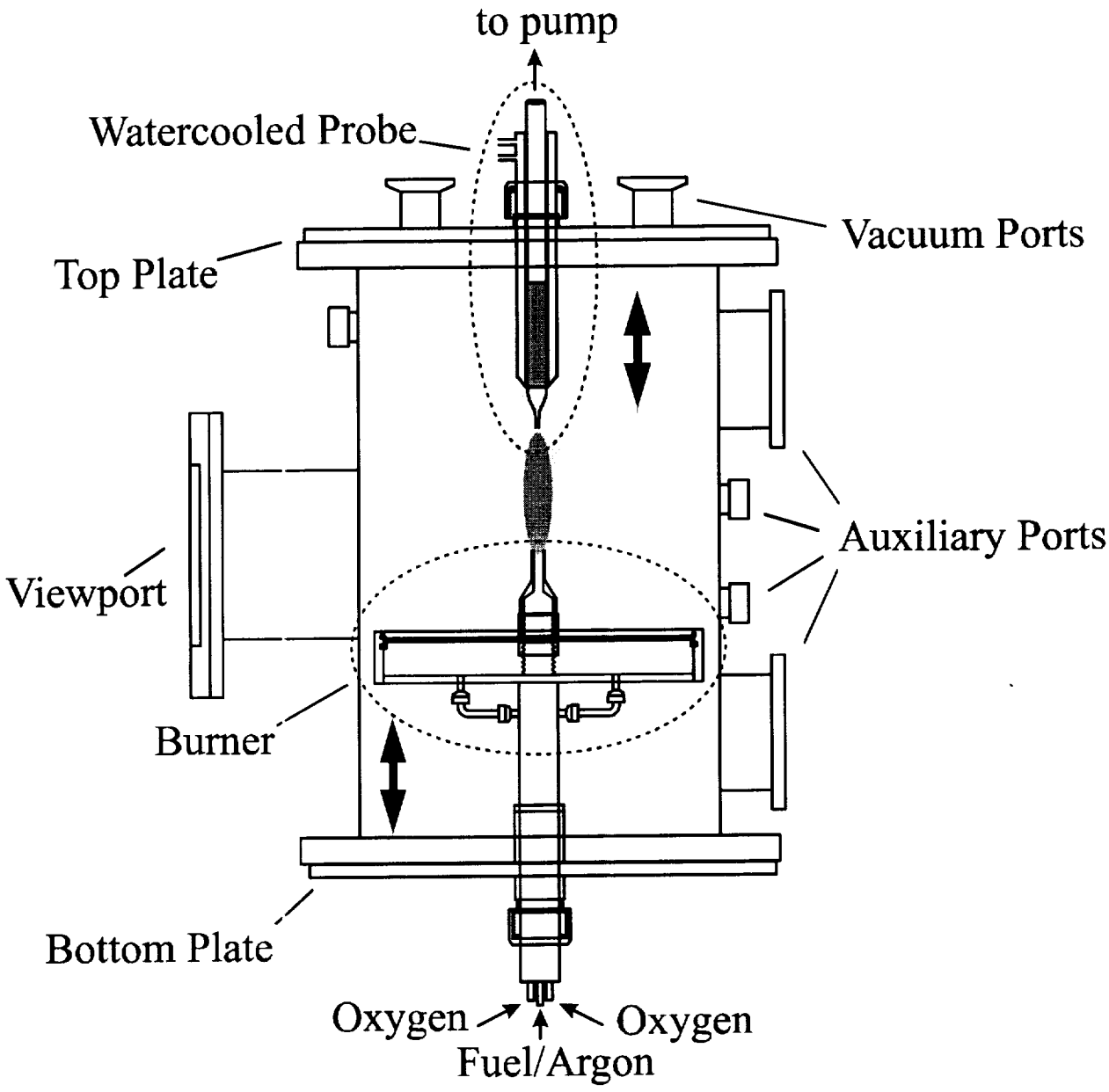

Figure 1: Experimental Setup

The cold gas velocity of the unburned benzene/argon mixture, v_u(fuel/Ar), was 820 or 840 cm/s and the dilution with argon, dil_{Ar}, was varied from 65 to 87.6 %. Oxygen was kept at a cold gas velocity, v_u(oxy), of 3.65 cm/s. The pressure, p, in the burning chamber was varied from 12 to 40 Torr.

A 10-mm-ID vertically-adjustable quartz microprobe with an orifice of 1.5 to 2 mm was used for sampling the flames. The probe was held in a watercooled jacket and operated at ~2 Torr. Condensable combustion products including polycyclic aromatic hydrocarbons (PAH), fullerenes, and soot, were collected on a preweighed filter system, consisting of a glass wool plug in an aluminum foil sleeve. Sampling times ranged from 1 to 5 minutes, and were limited by soot clogging the probe. More heavily sooting conditions than those studied here could not be measured. The noncondensable gas from the filter was collected in a graduated water column. The mass of the filter was measured after sampling to determine the amount of flame material collected. The filter was then submerged in toluene, ultrasonicated, and the solution was filtered through a 0.45 μm nylon filter and analyzed for fullerenes with a high performance liquid chromatograph (HPLC, Cosmosil Buckprep column, 4.6 x 250 mm with 1.0 ml/min toluene) with a VWD detector calibrated for C_{60} and C_{70}, using a wavelength of 330 nm.

Samples from different heights above the burner in the axial center of the flame were taken by changing the vertical positions of the burner and the probe. The ratio of the total mass of fullerenes to the total mass of condensable material and to the total volume of the noncondensable gas are used as parameters to characterize the fullerene production in the flames.

The maximum flame temperatures were determined with a calibrated pyrometer (Micro Optical Pyrometer 95C, The Pyrometer Instrument Co., Inc.) and corrected for a spectral

emissivity of 0.85, which gave an addition of ~20 K. Thermocouple pyrometry was not possible because of heavy soot deposition on the thermocouples in less than a second.

Soot particles and carbon nanostructures, including nanotubes and onions, were analyzed by high-resolution transmission electron microscopy (HRTEM). A small amount of the sonicated toluene mixture was diluted with additional toluene and again ultrasonicated. A few drops of the diluted mixture were deposited on an electron microscope grid and the toluene was allowed to evaporate prior to analysis. The grids consisted of a 200 mesh copper substrate on which a holey carbon film and a supporting polymeric substrate were deposited. The electron microscopes were operated at 200 keV with resolutions better than 0.2 nm. The curvatures, arc lengths, and diameters of carbon structures seen in the soot images were then quantified using a MatLab analysis tool described elsewhere [6].

Results

Fullerenes

The parameters of the flames studied are listed in Table 1. The HPLC analysis shows primarily C_{60} and C_{70} with small amounts of PAH, oxidized fullerenes, and higher fullerenes up to C_{96}. In all cases, C_{60} and C_{70} constitute over 95% of the mass of fullerenes analyzed by the chromatograph. Consequently, for data comparison, we used the mass of C_{60} and C_{70} relative to the total mass of condensable material as representative of the concentration of fullerenes. Table 1 shows the distance, h_{max}, from the fuel outlet to the probe inlet for the samples having the maximum percentage of fullerenes in the condensable material. Also shown are the maximum percentage of C_{60} and C_{70}, the maximum flame temperature, and the flame reference number used in later graphs.

Table 1: Flame parameters

p Torr	v_u(fuel/Ar) cm/s	dil_{Ar} % Ar	v_u(oxy) cm/s	h_{max} mm	$C_{60}+C_{70}$ mass %	T_{max} K	flame ref. #
20	840	66.5	3.65	84.5	2.97	1659	5
20	840	71.0	3.65	74.5	6.83	1689	4
20	840	76.0	3.65	61.5	5.13	1635	3
40	820	80.3	3.65	96.5	3.15	1694	10
40	820	82.8	3.65	88	3.73	1726	8
40	820	85.3	3.65	74	4.49	1754	11
40	820	87.6	3.65	69	4.86	1694	12
12	820	65.0	3.65	57	12.44	1599	13
12	820	67.5	3.65	53	12.40	1583	14

The highest soot concentration in diffusion flames is in the wings of a flame, where the radial fuel and oxygen concentration gradients are highest and the temperature is maximum. Further from the flame axis, the soot is consumed by oxidation. The flame wings collapse to one point at the tip of the stoichiometric surface, where the flame reaches its highest overall temperature: therefore, the axial concentration gradients of fuel, oxygen, and products including soot are similar to the radial gradients closer to the burner.

Results from three 20-Torr flames with different argon dilutions are shown in Fig. 2(a) and 2(b). The amount of C_{60} and C_{70} as a mass percent of the condensables is shown in Fig. 2(a) and the concentration of C_{60} and C_{70} in the cold sampled gas is shown in Fig. 2(b), both versus the height above the burner.

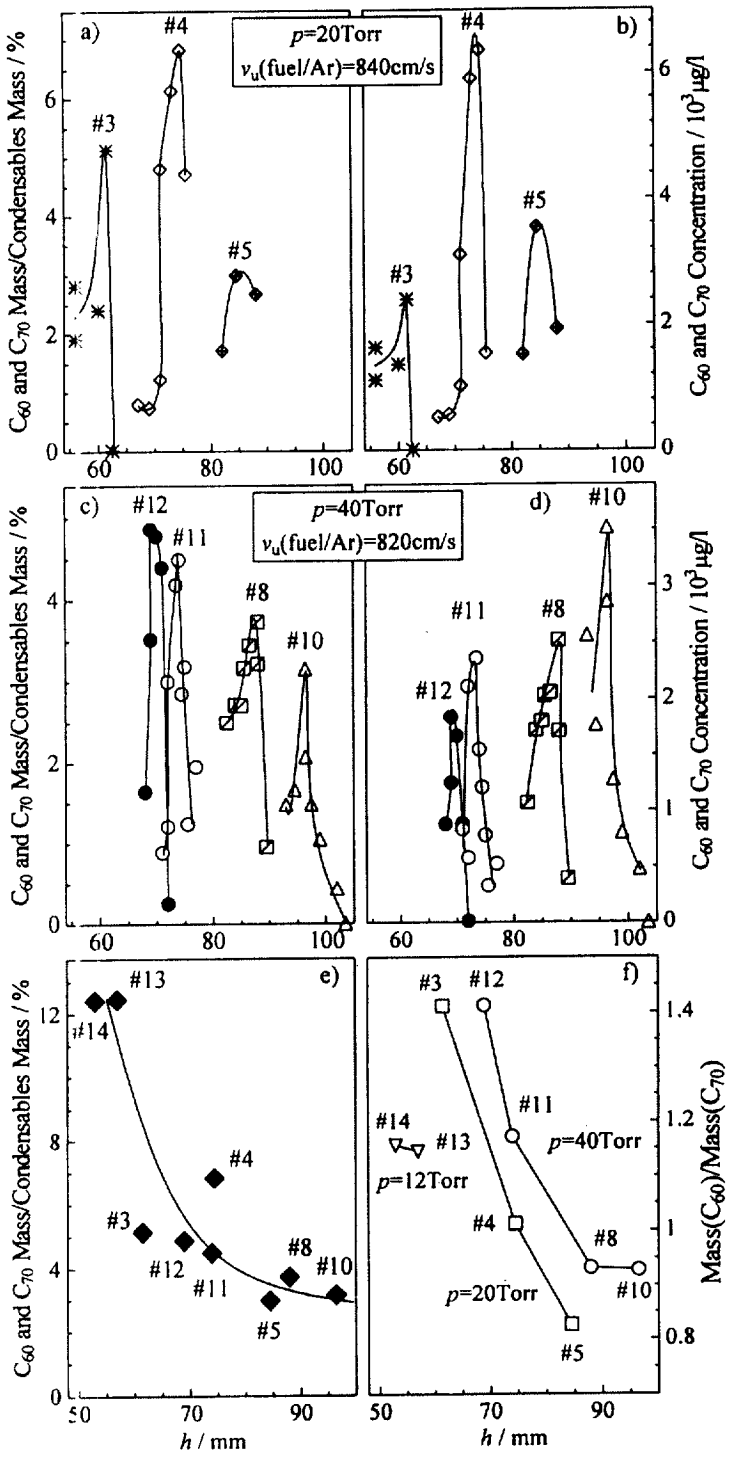

Fig. 2

Figure 2: Quantity of fullerenes C_{60} and C_{70} in the condensable material (a, c) and concentration of fullerenes C_{60} and C_{70} in the cold probed gas (b, d) from different heights above the burner in different flames, and maximum amount of fullerenes C_{60} and C_{70} (e) and mass ratio of C_{60} to C_{70} (f) in the condensable material at the height above the burner corresponding to maximum fullerene concentration in flames, at different pressures (p) and different argon dilutions (dil_{Ar}).

The highest concentration of fullerenes always occurred just above the visible stoichiometric surface of the flame, where the temperature maximum also occurs. Therefore, the locations of the maxima of the curves are indicative of the stoichiometric flame length. From Fig. 2(a) and 2(b) and Table 1, diluting the benzene with argon results in a shorter flame but not necessarily in a lower temperature and a higher fullerene percentage does not necessarily indicate a higher fullerene concentration. A decrease in the concentration of condensable material can be large enough to offset the increase in fullerene percentage. Estimation of the percentage of the carbon fed that is converted into fullerenes from the flame #4 data gives 0.5%. This value, for non-optimized conditions, is comparable to the largest value observed in premixed benzene flames [11,12].

Data for flames at 40 Torr (Fig. 2(c) and 2(d)) compared to those for 20 Torr (Fig. 2(a) and 2(b)) show that increasing pressure increases the flame length while decreasing the flame diameter, resulting in a more heavily sooting flame. In general, the percentage of fullerenes is lower at 40 Torr than at 20 Torr. For lower dilutions than those shown in Fig. 2(c) and 2(d), large soot concentrations at 40 Torr caused rapid probe clogging. With increasing dilution, the 40-Torr flames show an increase in the maximum percentage of fullerenes (Fig. 2(c)) and a decrease in the maximum fullerene concentration (Fig. 2(d)). Although measurements were taken at dilutions up to 87.6 %, where the temperature is lower than that of the next lower dilution, the peak in percentage of fullerenes is still higher. At lower dilutions, the concentration would be expected to decrease with decreasing dilution because the flame temperature goes down due to increased soot radiation. Such behavior is seen in premixed flames [11,12], where the concentration of fullerenes decreases with decreasing fuel dilution over a specified range of dilutions.

Two flames were studied at 12 Torr (Table 1). Consistent with the other results, the flames were shorter and the percentage of the fullerenes was higher than at 20 Torr.

The maximum percentage of fullerenes in the condensable material from the different flames decreases with increasing flame length in a strong relation as shown in Fig. 2(e). Shorter flames, which result from higher dilution or lower pressure, favor fullerenes over soot, possibly indicating fullerene consumption by soot as has also been suggested based on behavior seen in premixed flames [17]. This consumption should be slower for lower pressures and higher dilutions because of lower soot concentrations. The effect of a lower precursor concentration seems to be overwhelmed.

For each set of flames at different pressures, the mass ratio of C_{60} to C_{70} at the maximum fullerene concentration for each flame, increases with increasing dilution (Fig. 2(f)). However, unlike the fullerene percentage trend, this effect is pressure dependent.

Soot Structure Evolution

An example of an HRTEM micrograph of soot from flame #11 (75 mm) is shown in Fig. 3 (the white color in the images represents carbon layers or shells). The inset shows an enlarged area with closed shells. Significantly more ordered and more curved carbon layers or shells were seen in this study than in premixed benzene combustion [6].

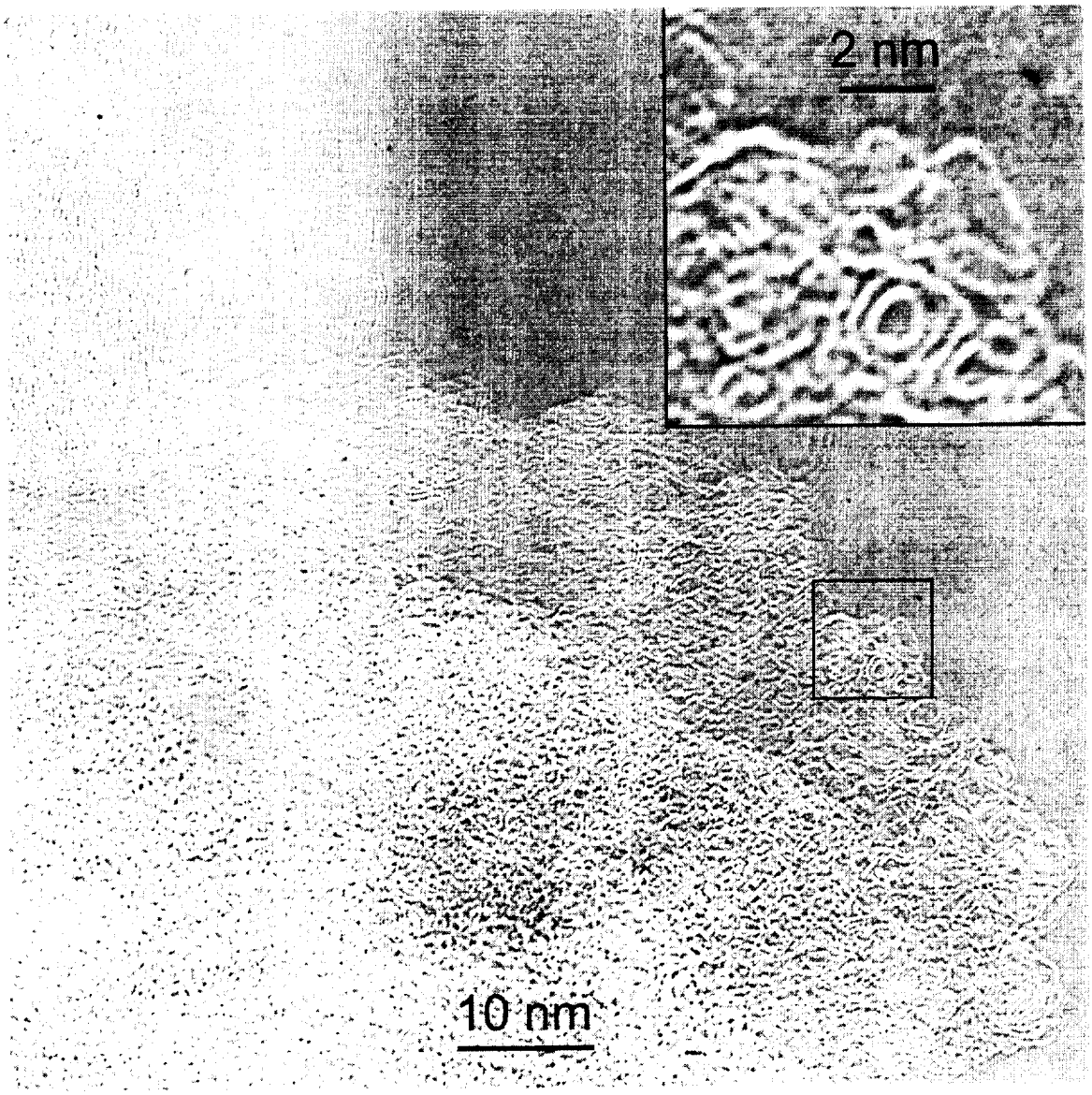

Figure 3: Representative HRTEM image of condensable material collected at h = 75 mm in flame #11 (p = 40 Torr, v_u(fuel/Ar) = 820 cm/s, v_u(oxy) = 3.65 cm/s, dil_{Ar} = 85.3%).

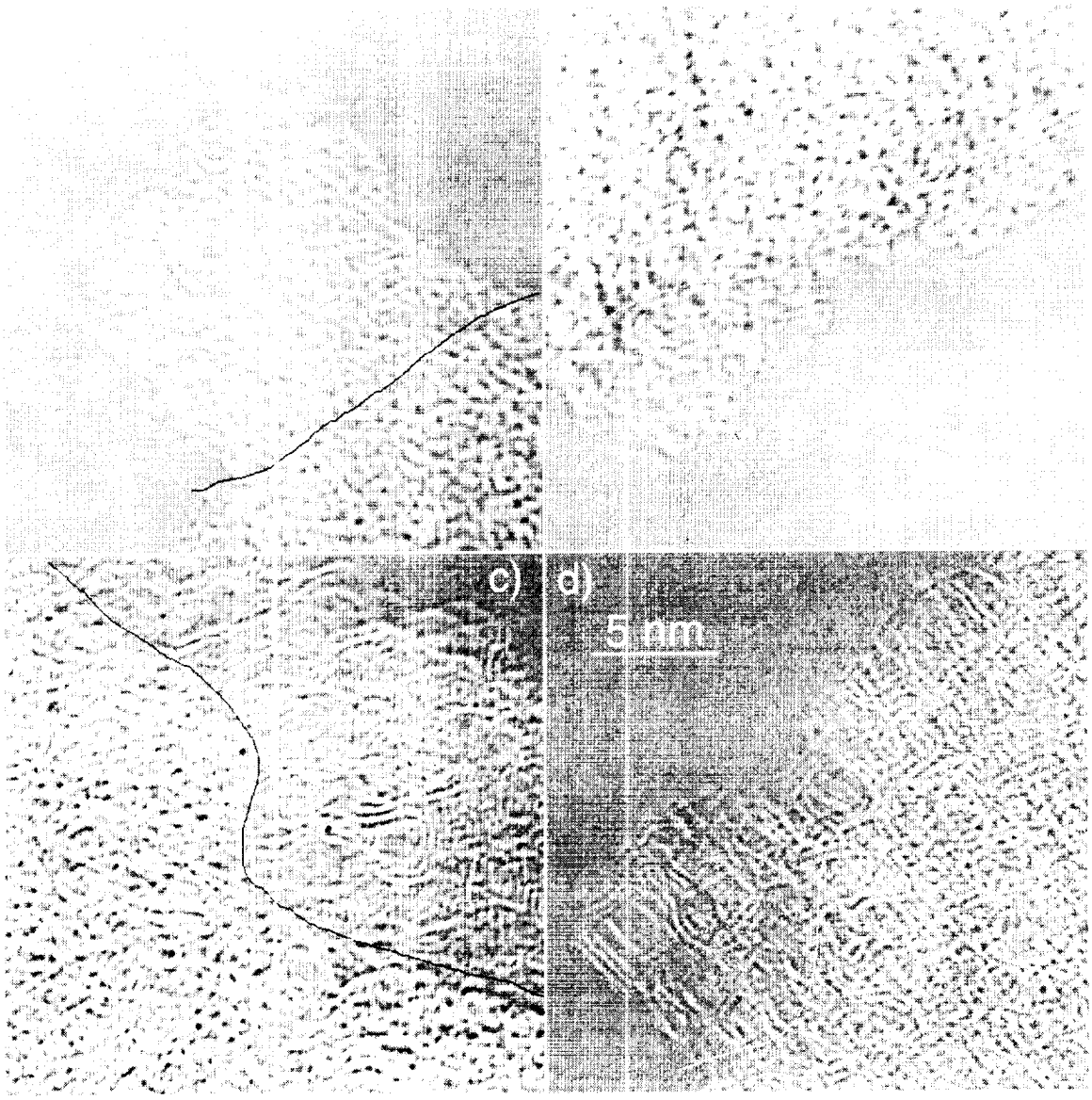

Figure 4: Representative counted material from soot collected at h = 72 mm (a), 74 mm (b), 75 mm (c), and 77 mm (d) in flame #11 (p = 40 Torr, v_u(fuel/Ar) = 820 cm/s, v_u(oxy) = 3.65 cm/s, dil_{Ar} = 85.3%).

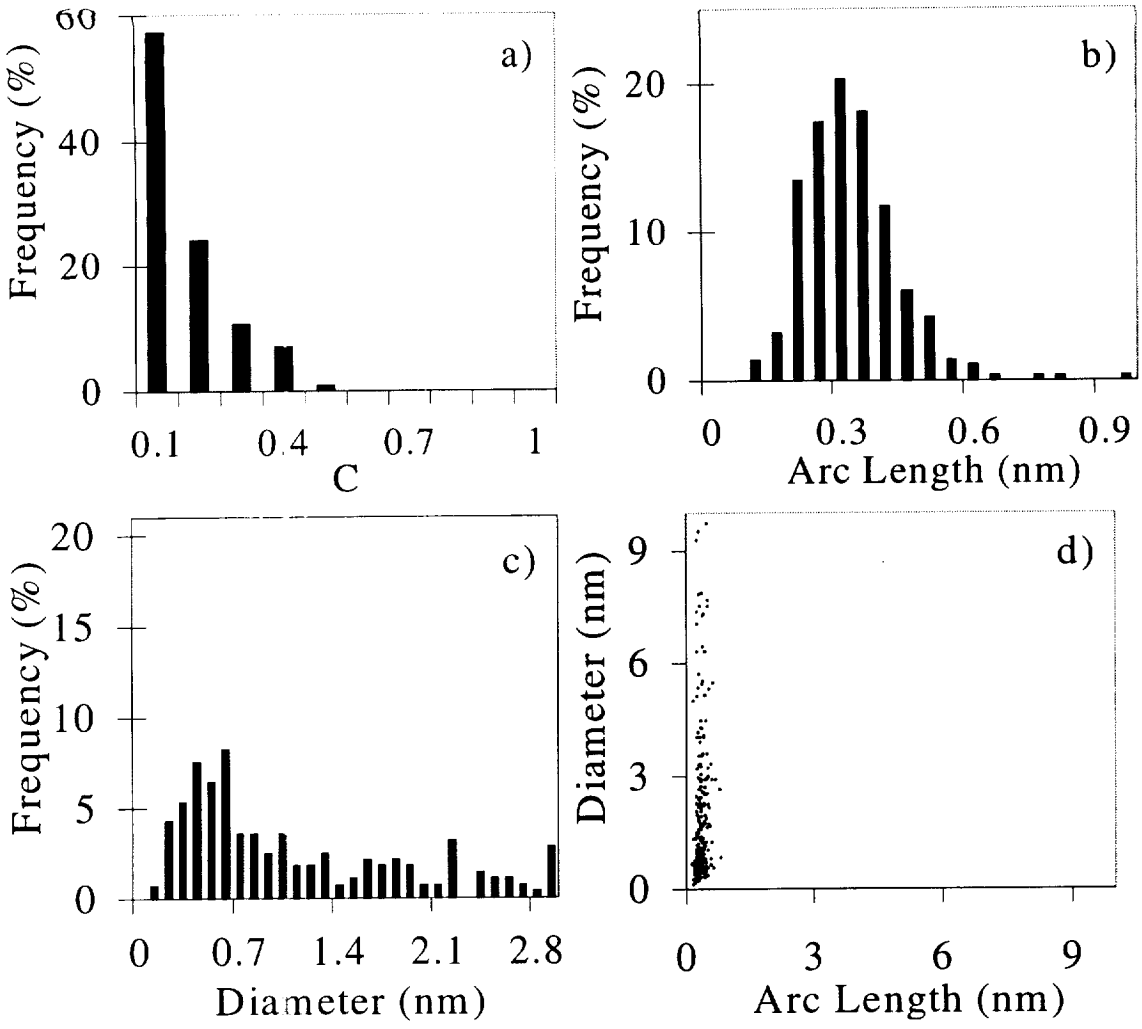

Figure 5: Normalized histograms of curvature (a), arc length (b), and diameter (c) and arc length vs. diameter scatterplot (d) of amorphous carbon material.

Figure 4 shows soot from four different heights above the burner that were used for the curvature analysis. Carbon structures along the periphery of the soot particles were analyzed quantitatively to determine the evolution of the structures with increasing height above the burner. Only the periphery of the particles was thin enough to allow for accurate measurements of the layers. The hand-drawn lines show the boundary between the outside area that was counted and the particle interior.

Two properties of the curved layers or shells, arc length (L) and diameter (D), were measured directly and used to calculate a non-dimensional parameter, curvature ($C = L/\pi D$). Values of C range from zero for a graphitic sheet to unity for a closed shell. Normalized histograms of each of these parameters and scatterplots of arc length versus diameter are shown for each of the four samples and amorphous carbon in Fig. 5-9. The truncation of the x-axes in these figures causes some of the histograms to sum to less than 100.

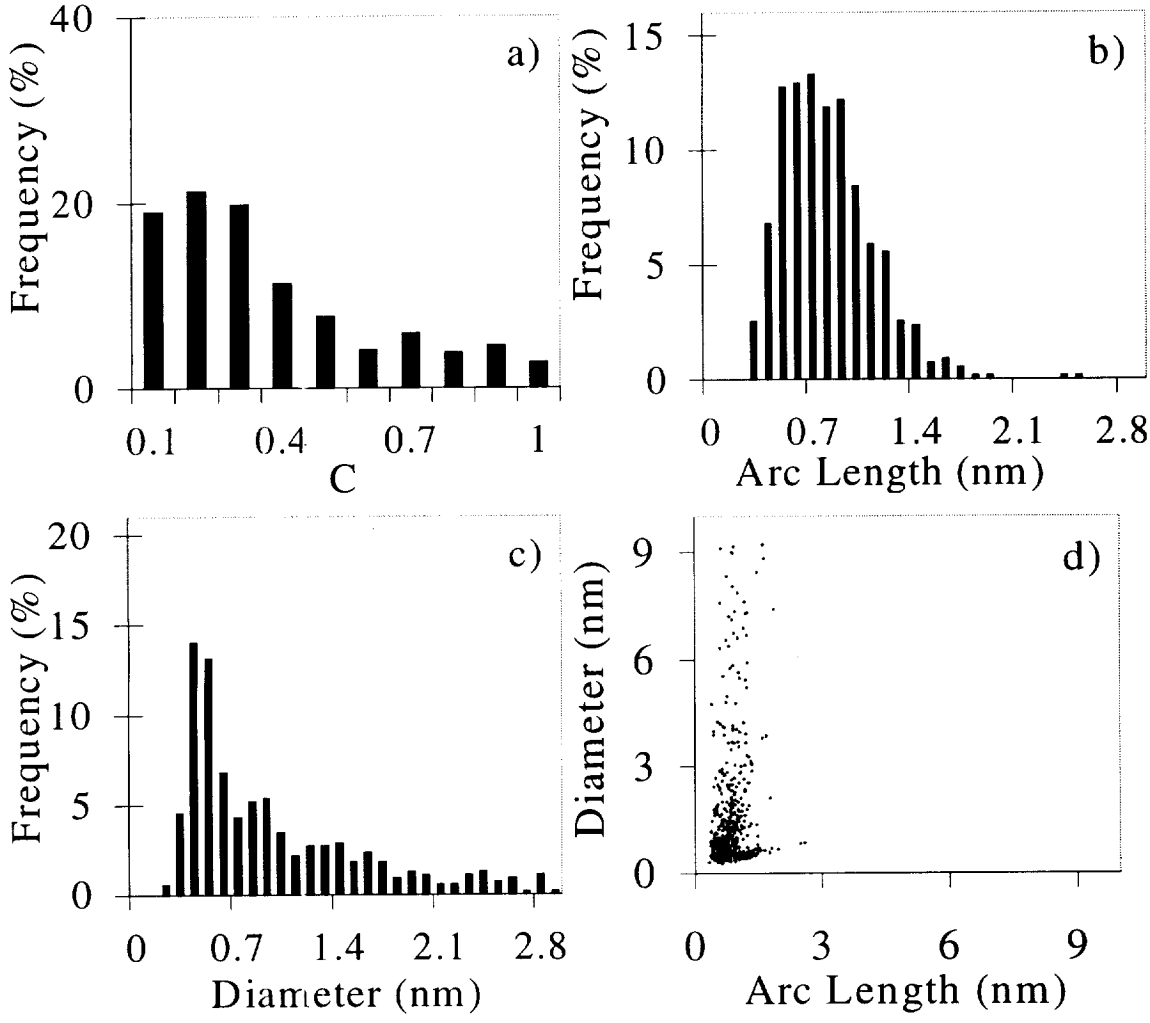

Figure 6: Normalized histograms of curvature (a), arc length (b), and diameter (c) and arc length vs. diameter scatterplot (d) of condensable material collected at h = 72 mm in flame #11 (p = 40 Torr, v_u(fuel/Ar) = 820 cm/s, v_u(oxy) = 3.65 cm/s, dil_{Ar} = 85.3%).

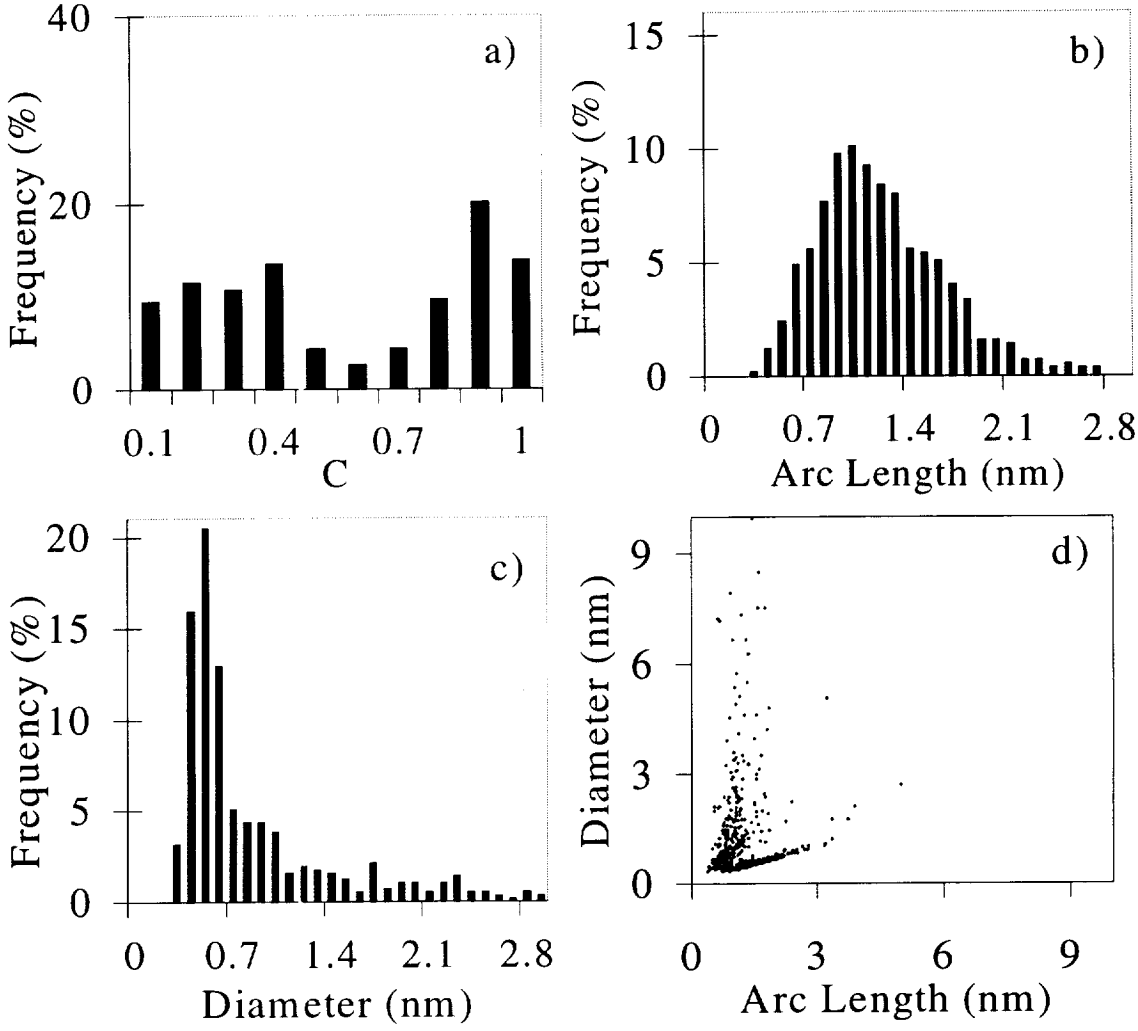

Figure 7: Normalized histograms of curvature (a), arc length (b), and diameter (c) and arc length vs. diameter scatterplot (d) of condensable material collected at h = 74 mm in flame #11 (p = 40 Torr, v_u(fuel/Ar) = 820 cm/s, v_u(oxy) = 3.65 cm/s, dil_{Ar} = 85.3%).

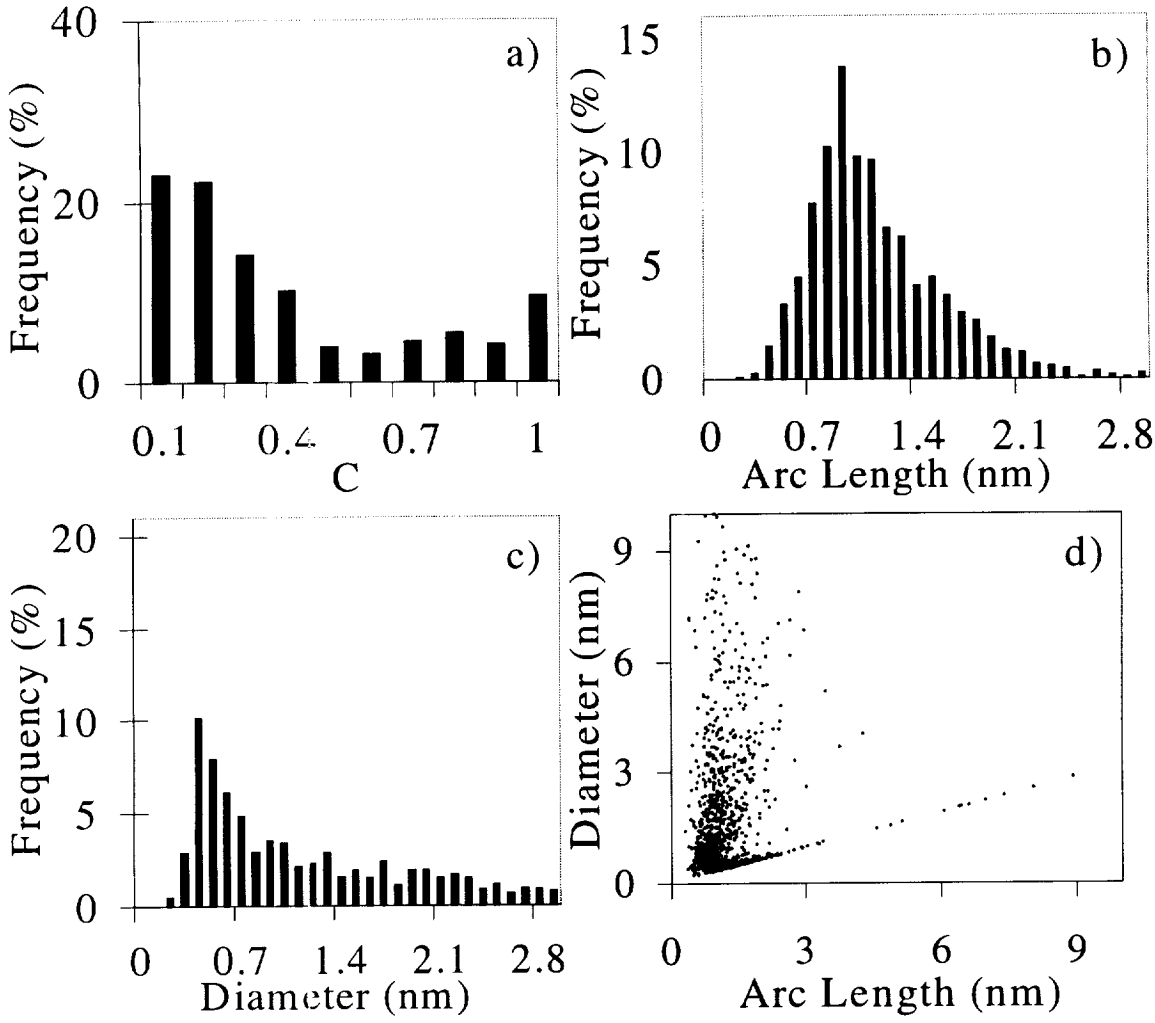

Figure 8: Normalized histograms of curvature (a), arc length (b), and diameter (c) and arc length vs. diameter scatterplot (d) of condensable material collected at h = 75 mm in flame #11 (p = 40 Torr, v_u(fuel/Ar) = 820 cm/s, v_u(oxy) = 3.65 cm/s, dil_{Ar} = 85.3%).

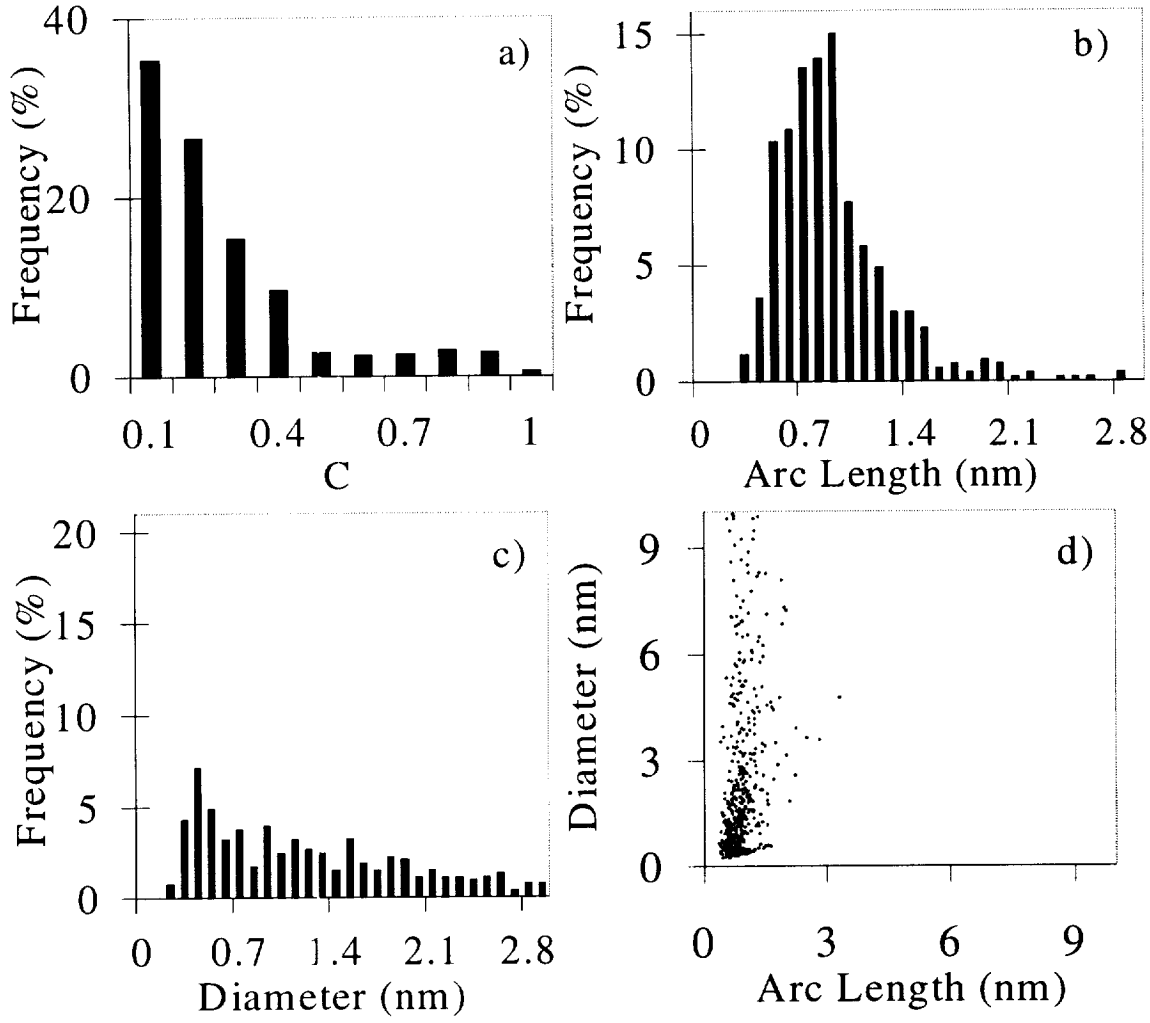

Figure 9: Normalized histograms of curvature (a), arc length (b), and diameter (c) and arc length vs. diameter scatterplot (d) of condensable material collected at h = 77 mm in flame #11 (p = 40 Torr, v_u(fuel/Ar) = 820 cm/s, v_u(oxy) = 3.65 cm/s, dil_{Ar} = 85.3%).

It can be seen that the structures in this amorphous carbon sample, compared to those of any flame sample, have very low curvatures, and are relatively short. The large diameters seen in the amorphous carbon are due to the relatively flat nature of the structures. As a consequence of the analysis method, the flatter of two structures with equal arc length will have a greater measured diameter.

A comparison of the curvature histograms in Fig. 5-9 (parts (a)) shows that curvature increases with distance until the fullerene maximum (74 mm), where it then decreases. This

indicates that the observed fullerene peak is also the peak for the generation of completely closed-shell structures. The histograms in parts (b) of the figures show a similar behavior in that arc lengths increase until a dropoff is observed after the fullerene maximum. The part (c) histograms show a decrease in diameter with increasing distance until the fullerene maximum, followed by an increase. The diameter peak is seen at 0.7 nm, the diameter of a C_{60} molecule, and highest at 74 mm, then becoming less pronounced after the fullerene maximum. In the scatterplots of parts (d), points that lie on the delineated lower boundary represent complete closed-shell structures. It appears that larger closed-shell structures are more prevalent with increasing distance until they practically disappear at 77 mm. Considering these trends collectively, it can be seen that the carbon structures in the soot become more curved and more closed until the fullerene peak, then change to flatter, smaller structures.

The sample images were examined qualitatively for the emergence of fullerenic nanostructures. Figure 10 shows a micrograph representative of the nanostructures from flame #13 at 61 mm, which consist of stacked layers of apparently fullerenic carbon, and include nanotubes, and highly ordered onion structures. The inset in Fig. 10 shows an enlarged onion-like closed-shell nanostructure. Similar structures have been seen in fullerene-forming premixed benzene flames [6,14,15,16].

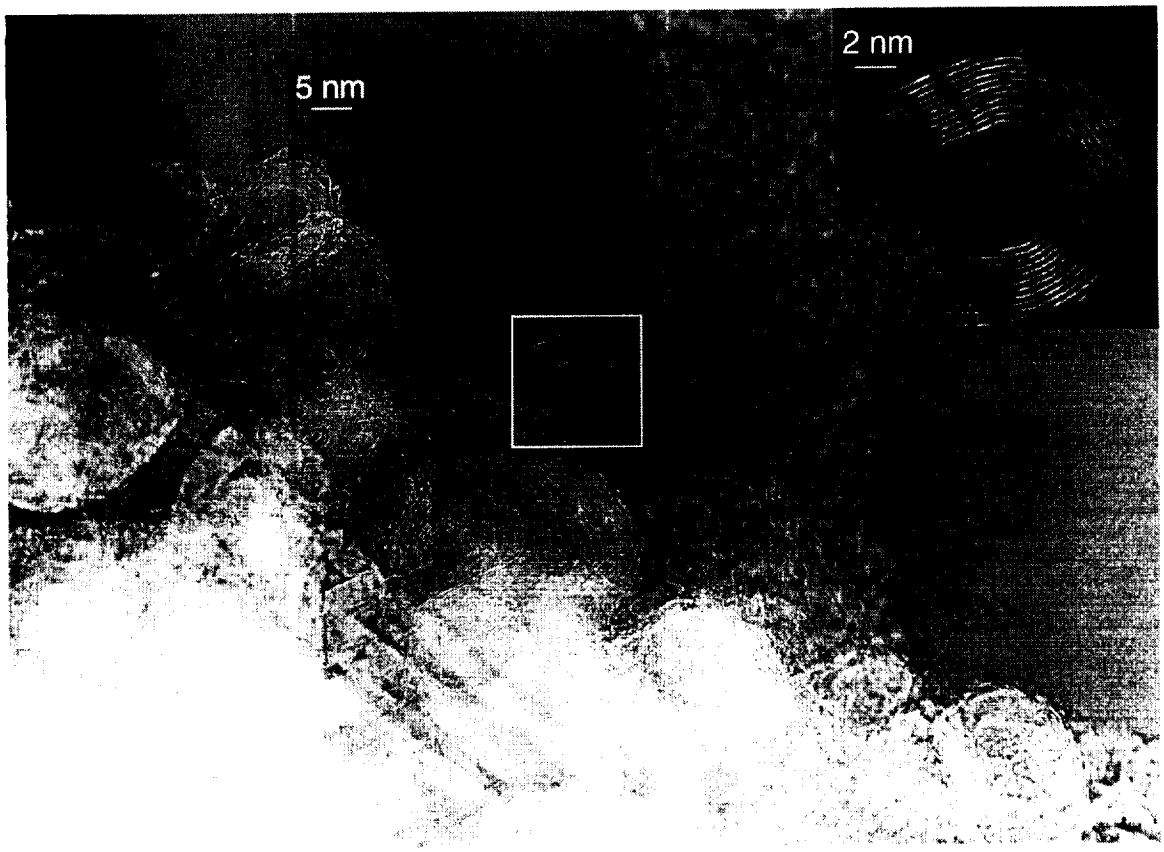

Figure 10: HRTEM image of fullerenic nanostructures in condensable material collected at h = 61 mm in flame #13 (p = 12 Torr, v_u(fuel/Ar) = 820 cm/s, v_u(oxy) = 3.65 cm/s, dil_{Ar} = 65.0%).

Discussion

Fullerenes

The elimination of CO from oxidized PAH is thought to be a source of five membered rings [18] in the structure of combustion generated PAH, which are precursors to fullerenes in flames [19,20,21]. However, the highest concentration of fullerenes is in the region of the flame where the precursor concentration is decreasing due to oxidation. Oxidation reactions are also responsible for the decomposition of the fullerenes at higher distances.

That the maximum fullerene percentage is at such high fuel dilutions as those seen here may indicate that fullerene consumption by soot is important. At 40 Torr (Fig 2(c) and (d)), the

percentage of fullerenes is highest at the highest dilution, but the temperature is lower compared to lower dilutions. The overall carbon concentration in the flame and soot formation decrease with increasing dilution. The lower soot concentrations at higher dilutions reduces radiative heat loss from the flame, partially offsetting the lower heat production due to less fuel. At the same time, the concentration of precursors for fullerenes, as well as soot, is decreasing but the flames with the lowest total concentration exhibit the highest fullerene percentage. Similarly, decreasing pressure lowers total soot and fullerene concentration but still raises the percentage of fullerenes. Associated with these effects is the observed strong correlation in which shorter flames yield higher percentages of fullerenes in the condensable material.

Although this provides a qualitative explanation for the appearance of a maximum rate of fullerene formation, a quantitative prediction for the optimal dilution is not yet possible. It is possible, however, to vary the percentage of fullerenes in the soot and the distribution between the fullerenes over a wide range by varying pressure, dilution, and cold gas velocity in the right combination.

Soot structure evolution

The electron microscope images show a soot microstructure that is different from samples collected from higher-pressure flames as well as low-pressure premixed flames [6]. Structures similar to those seen here have also been found in commercially-produced carbon black [22,23]. Quantitative analysis of the micrographs using the curvature parameter cited above indicates that carbon layers or shells in the soot become more curved, i.e., more fullerenic, with increasing distance in the flame up to the fullerene maximum, after which the curvature declines (Fig. 5-9). The arc length increases with distance, indicating growth to larger structures, while diameter

decreases, indicating increase of curvature of layers already present in the soot, or addition to the soot of smaller diameter fullerenic carbon. Together, these trends indicate that gas-phase-formed fullerenes are consumed by, and presumably incorporated into, the soot and nanostructures. This behavior is consistent with the hypothesis that fullerenes added to the soot from the gas phase are a source of the fullerenic structures, including closed shells, of around 0.7-nm diameter seen in the soot micrographs. The added fullerenes might also contribute, along with other polycyclic material in the soot, to the growth of larger curved layers indicated by the increase of arc length. The correspondence of the diminishing of the 0.7-nm diameter peak and the fullerene maximum is also consistent with the fullerene-addition hypothesis.

The quantity of nanotubes and onion-like structures (Fig.10) is higher than in premixed flames [6] where nanostructures are seen only at long residence times after oxygen depletion. In our flames, nanostructures appear soon after the stoichiometric flame surface where the maximum temperature occurs and the fullerenes and soot are being oxidized. Consequently, the time-scale for nanostructure formation in diffusion flames must be shorter than that for premixed combustion. It can be concluded that fullerenic nanostructures are formed after the fullerene peak where soot and fullerenes are being consumed by oxidation. The images appear to show nanostructure precursors that were being formed from the soot material.

Conclusions

The evolution of fullerenes, fullerenic soot material, and fullerenic nanostructures with increasing distance from the fuel outlet, as concluded by the findings in this study, can be summarized as follows:

- Prior to stoichiometric surface

- Pre-C_{60} incubation
- Presence of relatively flat soot structures
- Curvature of soot structures and concentration of C_{60}/C_{70} increasing with distance

• Just above stoichiometric surface

- Peak of C_{60}/C_{70} concentration
- Maximum temperature and soot structure curvature
- Presence of nanostructure precursor cells

• After stoichiometric surface

- Fullerenes consumed by oxidation and incorporation into nanostructures
- Curvature of soot structures and concentration of C_{60}/C_{70} decreasing with distance
- Appearance of fullerenic nanostructures.

Acknowledgements

Participants in this research in addition to the principal investigator were Anish Goel, Peter Hebgen, Lenore C. Rainey and John B. Vander Sande.

References

[1] Kroto, H.W., Heath, J.R., O'Brien, S.C., Curl, R.E., Smalley, R.E., *Nature* **318**: 162 (1985).

[2] Iijima, S., *Nature* **354**: 56 (1991).

[3] Ugarte, D., *Carbon* **33**: 989 (1995).

[4] Howard, J.B., Chowdhury, K.D., and Vander Sande, J.B., *Nature* **370**: 603 (1994).

[5] Chowdhury, K.D., Howard, J.B., and Vander Sande, J.B., *J. Mater. Res.* **11**: 341 (1996).

[6] Grieco, W.J., Howard, J.B., Rainey, L.C., Vander Sande, J.B., *Carbon* **38**: 597 (2000).

[7] Werner, H., Herein, D , Blöcker, J., Henschke, B., Tegtmeyer, U., Schedelniedrig, T., Keil, M., Bradshaw, A.M., Schlogl, R. *Chem. Phys. Lett.* **194**: 62 (1992).

[8] Gerhardt, P., Löffler, S., and Homann, K.-H., *Chem. Phys. Lett.* **137**: 306-310 (1987).

[9] Gerhardt, P., Löffler, S., and Homann, K.-H., *Proc. Combust. Inst.* 22: 395 (1989).

[10] Howard, J.B., McKinnon, J.T., Makarovsky, Y., and Lafleur, A.L., and Johnson, M.E., *Nature* **352**: 139 (1991).

[11] Howard, J.B., McKinnon, J.T., Johnson ,M.E., Makarovsky, Y., and Lafleur, A.L., *J. Phys. Chem.* **96**: 6657 (1992).

[12] Howard, J.B., Lafleur, A.L., Makarovsky, Y., Mitra, S., Pope, C.J., and Yadav, T.K., *Carbon* **30**: 1183 (1992).

[13] Richter, H., Labrocca, A.J., Grieco, W.J., Taghizadeh, K., Lafleur, A.L., and Howard, J.B., *J. Phys. Chem. B* **101**: 1556 (1997).

[14] Anacleto, J.F., Boyd, R.K., Pleasance, S., Quilliam, M.A., Howard, J.B., Lalfeur, A.L., and Makarovsky, Y., *Can. J. Chem.* **70:** 2558 (1992).

[15] Anacleto, J.F., Quilliam, M.A., Boyd, R.K., Howard, J.B., Lalfeur, A.L., and Yadav, T.K., *Radid Commun. Mass Spectrom.* **7**: 229 (1993).

[16] Richter, H. Hernadi, K., Cauano, R., Fonseca, A., Migeon, H.-N., Nagy, J.B., Schneider, S., Vandooren, J., and Van Tiggelen, P. J., *Carbon* **34:** 427 (1996).

[17] Grieco, W.J., Lafleur, A.L., Swallow, K.C., Richter, H., Taghizadeh, K., and Howard, J.B., *Proc. Combust. Inst.* 27: 1669 (1998).

[18] Bittner, J.D., and Howard, J.B., *Proc. Combust. Inst.* 18: 1105 (1981).

[19] Ahrens, J., Bachmann, M., Baum, T., Griesheimer, J. Kovacs, R., Weilmünster, P., and Homann, K.-H., *Int. J Mass Spectrom. Ion Processes* **138:** 133 (1994).

[20] Pope, C. J., Marr, J. A., and Howard, J. B., *J. Phys. Chem.* **97:** 11001 (1993).

[21] Lafleur, A.L., Howard, J.B., Marr, J.A., and Yadav, T., *J. Phys. Chem.* **97:** 13539 (1993).

[22] Donnet, J.B., *Rubber Chem. Technol.* **71**: 323 (1998).

[23] Donnet, J.B., Wang, T.K., Wang, C.C., Monthioux, M., Johnson, M.P., Norman, D.T., Wansborough, R.W., and Bertrand, P., *KGK Kautschuk Gummi Kunststoffe* Hüthig GmbH, Hiedelberg, 1999, p. 340.